Regions of Interest in the Venous Sinuses as Input Functions for Quantitative PET

Lindi M. Wahl, Marie-Claude Asselin and Claude Nahmias

Theoretical Biology, Institute for Advanced Study, Princeton, New Jersey; Department of Physics and Astronomy, McMaster University, Hamilton, Ontario; and Department of Nuclear Medicine, McMaster University Medical Center, Hamilton, Ontario, Canada

As clinical PET becomes increasingly available, quantitative methods that are feasible in busy clinical settings are becoming necessary. We investigated the use of intracranial blood pools as sources of an input function for quantitative PET. **Methods:** We studied 25 patients after the intravenous injection of [^{18}F]6-fluoro-L-m-tyrosine and compared sampled blood time-activity curves with those obtained in small regions of interest (ROIs) defined in the blood pools visible in the PET images. Because of the comparatively large dimensions of the blood pool at the confluence of the superior sagittal, straight and transverse sinuses, a venous ROI input function was chosen for further analysis. We applied simple corrections to the ROI-derived time-activity curves, deriving expressions for partial volume, spillover and partition of tracer between plasma and red blood cells. The results of graphic and compartmental analysis using both sampled [$C_s(t)$] and ROI [$C_r(t)$] venous input functions for each patient were compared. We also used an analytic approach to examine possible differences between venous and arterial input functions in the cerebral circulation. **Results:** $C_r(t)$ peaked significantly earlier and higher than $C_s(t)$ in this patient population, although the total integral under the curves did not differ significantly. We report some apparent differences in the results of modeling using the two input functions; however, neither the graphically determined influx constant, K_i, nor the model parameter that reflects presynaptic dopaminergic metabolism, k_3, differed significantly between the two methods. The analytic results suggest that the venous ROI input function may be closer to the arterial supply of radiotracer to the brain than arterialized venous blood, at least in some patient populations. **Conclusion:** We present a simple method of obtaining an input function for PET that is applicable to a wide range of tracers and quantitative methods and is feasible for diagnostic PET imaging.

Key Words: PET; input function; quantitation; clinical PET

J Nucl Med 1999; 40:1666–1675

One of the key strengths of PET is the ability to perform quantitative analysis, a feature that has been used extensively to determine in vivo cerebral blood flow, blood volume and the rates of transport, binding or metabolism of an increasing number of radiotracers (*1,2*). In many of these techniques, the accurate characterization of an input function, usually the time course of the radiotracer in the circulation, is a prerequisite for accurate quantitation (*3–5*). Although arterial sampling remains the gold standard input function for PET, the technical demands and invasiveness of this procedure have lead several groups to investigate alternative input functions, particularly in clinical settings. Arterialized venous input functions (*6*) have now been used extensively, and the number of blood samples may be reduced by several methods (*3,7,8*), usually through the use of population-based input functions (*9,10*). The continuous sampling of expired air has been used as an input function to determine local cerebral blood flow (*11*), and the use of a nonreceptor or nonspecific region of cerebral tissue has been elegantly characterized as an input function for receptor-binding studies (*12–14*). The use of a region of interest (ROI) within the left ventricle is now well established for cardiac studies (*15*), and this approach has recently been applied to studies of the brain by repositioning patients during the scanning interval (*16*). Although the rationale for avoiding arterial cannulation in a research setting has been questioned (*17*), these alternatives to arterial punctures have attracted renewed interest as clinical, quantitative PET becomes increasingly available (*10,18*).

The improved resolution and sensitivity of current tomographs led us to investigate the use of intracranial blood pools as input functions for quantitative PET, an approach that has been validated for other imaging modalities (*19,20*) and that has recently been suggested for the study of local cerebral glucose metabolism using PET (*18*). We describe this experience with 25 patients for whom blood and tissue time-activity curves were obtained simultaneously from the PET images. We chose the tracer [^{18}F]6-fluoro-L-m-tyrosine (FmT) (*21,22*) for this study because of the large clinical population available at our institution, but the method presented here is applicable to a wide range of PET radiopharmaceuticals. We estimate simple partial volume and spillover corrections for the blood time-activity curves. We consider the general case when the tracer does not equilibrate rapidly between the plasma and the red blood cells. We compare the resulting input functions with the input function in current clinical use at our institution, direct venous sampling. Finally, we use an analytic approach to examine possible differences between venous and arterial input functions in the cerebral circulation.

Received Jul. 31, 1998; revision accepted Apr. 9, 1999.

For correspondence or reprints contact: Claude Nahmias, PhD, Nuclear Medicine, HSC-1P, McMaster University Medical Center, 1200 Main St. W., Hamilton, Ontario, Canada L8N 3Z5.

MATERIALS AND METHODS

Standard Clinical Procedure

We examined 25 patients (16 men, 9 women; mean age 53 ±14 y) using our routine clinical procedure for investigating cerebral dopaminergic function with PET. These patients were referred for a variety of clinical reasons, involving differential diagnoses of Parkinson's disease, cortical basal ganglia degeneration and other movement disorders. Patients were asked to refrain from taking all medication 24 h before scanning and were studied after an overnight fast. Patients were examined by either an ECAT 953 (n = 8) or ECAT ART (n = 17) positron tomograph (CTI PET Systems, Knoxville, TN) after the intravenous injection of 185–370 MBq FmT. The head was positioned with the orbitomeatal line perpendicular to the gantry and was immobilized in a head holder; room light and ambient noise were kept to a minimum. Patients were scanned for 12 frames at 10 s per frame, for 6 frames at 30 s per frame and for 23 frames at 300 s per frame for a total of 2 h. Attenuation correction was calculated from a manually positioned ellipse in each of the axial planes: 47 overlapping planes covering a 15-cm field of view in the ECAT ART or 31 overlapping planes covering 10 cm in the ECAT 953. The last 6 frames (30 min) of the study were summed and ROIs were drawn manually around the left and right striata and the occipital lobe. The time course of radioactivity in these regions, in bequerels per cubic centimeter, was then obtained for the entire dynamic study (41 frames) for each patient. To express ROI time courses as fractions of injected dose, these concentrations may be normalized by the dose injected, as determined by the dose calibrator (CRC-12; Capintec Instruments Inc., Ramsey, NJ).

Arterialized venous blood samples were taken throughout each study, every 20 s for the first 3 min, every 30 s up to 5 min, every 2.5 min up to 20 min and then at 25, 30, 40, 50, 60, 75, 90, 105 and 120 min. These samples were spun for 5 min in a centrifuge, and the radioactivity in 1 mL plasma was then counted in a NaI (Tl) well counter (Minaxi γ; Packard Instruments Co., Downers Grove, IL). The counts reported by the well counter were decay corrected to the time of injection and then were normalized to percentage injected (%ID) dose by counting three 1-mL samples of a known mass fraction of the dose, diluted in a 1-L standard. The normalized time course of total plasma radioactivity will be referred to as the sampled venous input function [$C_s(t)$].

We defined the time course of the partition of FmT between plasma and red blood cells in 5 patients. For each blood sample, we counted separately 1 mL plasma and 1 mL whole blood in which the cells had been lysed by the addition of a small amount of saponin. We also measured the hematocrit in each sample.

Plasma samples at 10, 20, 50, 90 and 120 min were analyzed for labeled metabolites of FmT by high-pressure liquid chromatography as described (*23*). We obtained the time course of radioactivity attributable to FmT (the FmT fraction) by fitting a double exponential function to the fraction of FmT determined at each of these times. We then obtained the sampled FmT input function [$\mathscr{C}_s(t)$] by multiplying the time course of total plasma radioactivity by this FmT fraction. At our institution, we routinely use the time course of circulating FmT estimated in this way as an input function for both graphic and compartmental analyses, providing quantitative assessments of dopaminergic function (such as an influx constant) to the reporting or referring physicians (or both).

Region of Interest for Venous Input Function

The first several frames of each study were summed to obtain an image of the blood pool within the field of view; we initially varied the summation time to several values between 30 s and 2 min. In one study, we were able to use an MR venogram to confirm our interpretation of the vascular anatomy revealed by PET and to verify the position of the ROIs. The venogram was obtained by a 1.5-T Signa Imager (General Electric Medical Systems, Milwaukee, WI) using a standard pulse sequence. For several patients, a large number (up to 30) of ROIs were defined on the summed images, with varying size, shape and position, for both venous and arterial blood pools. After comparing these initial results, we chose to use a summed image of the first 6 frames (1 min) of the study and to define small (3.5- to 5.5-mm radius) circular ROIs over several planes in this image at the confluens sinuum, the confluence of the superior sagittal, straight and transverse sinuses. We defined ROIs at the confluens sinuum on between two to five successive planes, and therefore we covered a total of axial depth of 0.6–1.6 cm. A threshold value of 50% of the peak activity in the sinuses was used to guide the placement of the ROIs. The small range allowed in the ROI radius and number was due in part to differences in reconstructed pixel size and slice thickness on the two tomographs and in part to interobserver variation in manually defining the ROIs.

The time course of radioactivity in these venous ROIs was obtained for the entire dynamic study for each patient, and the data for ROIs on successive planes were averaged. The resulting time course, in becquerels per cubic centimeter, has been automatically corrected during reconstruction for detection efficiency, scatter, attenuation and decay in the same way that data from the striatal and occipital ROIs have been corrected. Data from the venous ROIs correspond to the measured concentration of radioactivity in whole blood, at the confluens sinuum, at each time point, $C_m(t)$.

We applied two further corrections to the input function obtained using this method. First, we performed a simple correction for partial volume, the effect of imaging an anatomic structure that fills only a fractional volume of some of the voxels in the ROI, and the spillover effect caused by the finite resolution of the tomograph (*24*). These effects can be corrected simultaneously through the use of a recovery coefficient, f; the recovery coefficient describes the fraction of "true" counts in the physical volume circumscribed by the ROI that is recovered by, or attributed to, the voxels of the ROI after reconstruction. The contribution of radioactivity in the tissue surrounding the ROI is weighted by (1 − f), such that:

$$C_m(t) = fC_w(t) + (1 - f)C_o(t),$$

where $C_m(t)$ is, again, the measured concentration time course, and $C_w(t)$ is the true concentration time course in whole blood. We used the occipital ROI, $C_o(t)$, to give an estimate of the concentration time course in surrounding tissue. Rearranging, we find that the concentration time course in whole blood is given by:

$$C_w(t) = [C_m(t) - C_o(t)]/f + C_o(t). \qquad \text{Eq. 1}$$

Equation 1 clarifies that the correction for both fractional pixel volume and spillover effects (referred to later as the partial-volume correction) is only applied to the difference between the measured activity in the region, $C_m(t)$, and the activity in the surrounding area.

The tomographs we used have been well characterized, with spatial resolutions of 6 mm (full width at half maximum [FWHM]) in three dimensions. To estimate the value of the recovery

coefficient, we simulated circular vessels with radii between 1 and 15 mm, centered on a 50 × 50 mm grid of 0.1-mm pixels. Pixels within these regions were arbitrarily assigned activities of 1, whereas surrounding pixels had 0 activity. The grid was then smoothed by a two-dimensional Gaussian operator with a FWHM of 6 mm (*25*). Circular ROIs were centered on the grid with radii between 1 and 35 mm, and the mean activity per pixel within the ROI was calculated. This value gives an estimate of f for regions of different radii drawn around a vessel of a given radius. To verify this analytic correction, we imaged glass tubes with internal radii of 2, 3, 3.85, 6.25 and 13.25 mm, each containing a solution of 62,900 Bq ^{18}F per cubic centimeter. Each tube was scanned for 5 min and was reconstructed using a ramp filter (cutoff frequency 0.5 Hz) and calculated attenuation correction. Circular ROIs with radii between 1 and 31 mm were centered over these vessels, and counts recovered were compared with the known concentration of ^{18}F in the solution.

Second, to obtain the concentration time course of radioactivity in plasma, we corrected for the fraction of radioactivity in whole blood that is from plasma. In general, this is given by:

$$C_r(t) = \frac{1 - H(1 - e^{-at})}{(1 - H)} C_w(t), \qquad \text{Eq. 2}$$

where H is the hematocrit, and a is the equilibration time constant. Note that if a is large, equilibrium is reached rapidly and $C_r(t) \approx C_w(t)$. On the other hand, if a is small, equilibrium is never reached, and $C_r(t) \approx C_w(t)/(1 - H)$.

The time course of radioactivity determined from the venous ROI can then be normalized to %ID to obtain $C_r(t)$ in units of fraction of injected dose. In the same way that the sampled input function is corrected for peripheral metabolism of the tracer, $C_r(t)$ can be multiplied by the FmT fraction to obtain $\mathcal{C}_r(t)$, the ROI input function for FmT.

Comparison of Input Functions

We examined the peak height, time to peak and total integral under both the sampled and the ROI plasma input functions, computing mean and SD and using two-tailed paired *t* tests to check for significant differences between the two distributions. We also computed average $C_s(t)$ and $C_r(t)$ for all patients, shifting the input functions such that peak times for all patients were aligned, to minimize the smoothing effect of averaging curves that peak at different times.

Given the measured time course of radioactivity at the confluens sinuum, we wished to estimate the time course in the internal carotid artery. The transit of tracer substances through brain tissue has been well characterized in the literature (*26–28*). In particular, values of the appropriate permeability surface area products and distribution volumes for the transit of a large number of large neutral amino acids between the carotid artery and jugular vein have been determined (*29*). To evaluate the arterial-venous impulse response for a given tracer from these parameters (Eq. 23 [*27*]), it was necessary to provide a reference function describing the arterial-venous transfer function for an inert, nondiffusable tracer. To describe this reference function, we used the model proposed by Knudsen et al. (Eq. A1 [*28*]), with parameter values determined for Na^+ (Table 1 [*28*]), the reference substance used for studies of L-phenylalanine and other amino acids (*28,29*). As an approximation of the arterial-venous transfer function for FmT, we used this reference function and the well-mixed model proposed by Knudsen et al. (*27*), with parameter values determined for tyrosine (Table 1 [*29*]).

To apply the transfer function for tyrosine computed in this way to our measured data, we fit the mean $C_r(t)$ to a smooth function (by Nelder-Mead simplex):

$$C_r(t) = \frac{M'}{\sqrt{4\pi D't}} \exp\left(\frac{-(1 - v't)^2}{4D't}\right). \qquad \text{Eq. 3}$$

This function describes the dilution of a bolus input as it travels through a thin tube (*30*) and depends on three parameters, each normalized to the distance between the injection point and the sampling point, x_0: the amount injected, $M' = M/x_0$; the diffusion of the substance in the medium, $D' = D/x_0^2$; and the speed of the bolus as it travels through the medium, $v' = v/x_0$. (A gamma variate was also fit to the mean $C_r(t)$ but the results were not visibly different.) The smooth fit to the mean input function was then deconvolved with the computed arterial-venous transfer function for tyrosine, yielding an estimate of the time course of radioactivity in the carotid artery. In this way, we estimated some of the possible differences between the time courses of radioactivity in the arterial and venous blood in the brain.

Finally, we evaluated the effect of using either $\mathcal{C}_s(t)$ or $\mathcal{C}_r(t)$ as input functions for both graphic and compartmental analysis, using the time course of radioactivity in the striatum for each patient as the tissue compartment. We performed the graphic method proposed by Wong et al. (*31*) and a simple two-compartment, three-rate-constant model (*23*). Note that both the sampled and the ROI plasma input functions were corrected for FmT fraction as described previously before being used as inputs to the analyses. The slope (influx constant, K_i), intercept and rate constants that provided the best fit to the measured data were determined using a Nelder-Mead simplex search method. We examined correlation between parameters calculated using the two methods and performed two-tailed paired *t* tests to check for significant differences between parameter values.

RESULTS

We found the images obtained by summing the first minute of scanning to be remarkably similar among patients; an example is shown in Figure 1A. Transaxial and sagittal sections clearly show the transverse and superior sagittal sinuses, respectively; the confluence of these sinuses is easily identifiable on the PET images and is visible in the coronal section (center panel). The graph (Fig. 1B) illustrates the time courses of radioactivity in several ROIs shown in transaxial sections (Fig. 1C); these ROI time courses have not been corrected for partial volume or partition. Note that the time to peak rarely differs for different areas within the blood pools of a single patient, whereas peak height and peak width can differ more noticeably. The maximum peak height for the ROIs defined in the venous blood pool is 41% higher than the peak in the internal carotid artery. Given the wide range of blood vessel diameters throughout the brain, this variation is most likely associated with partial-volume effects.

Figure 2A illustrates the magnitude of the analytically derived recovery coefficient for circular vessels with 1- to 15-mm radii, sampled by circular ROIs with 1- to 15-mm

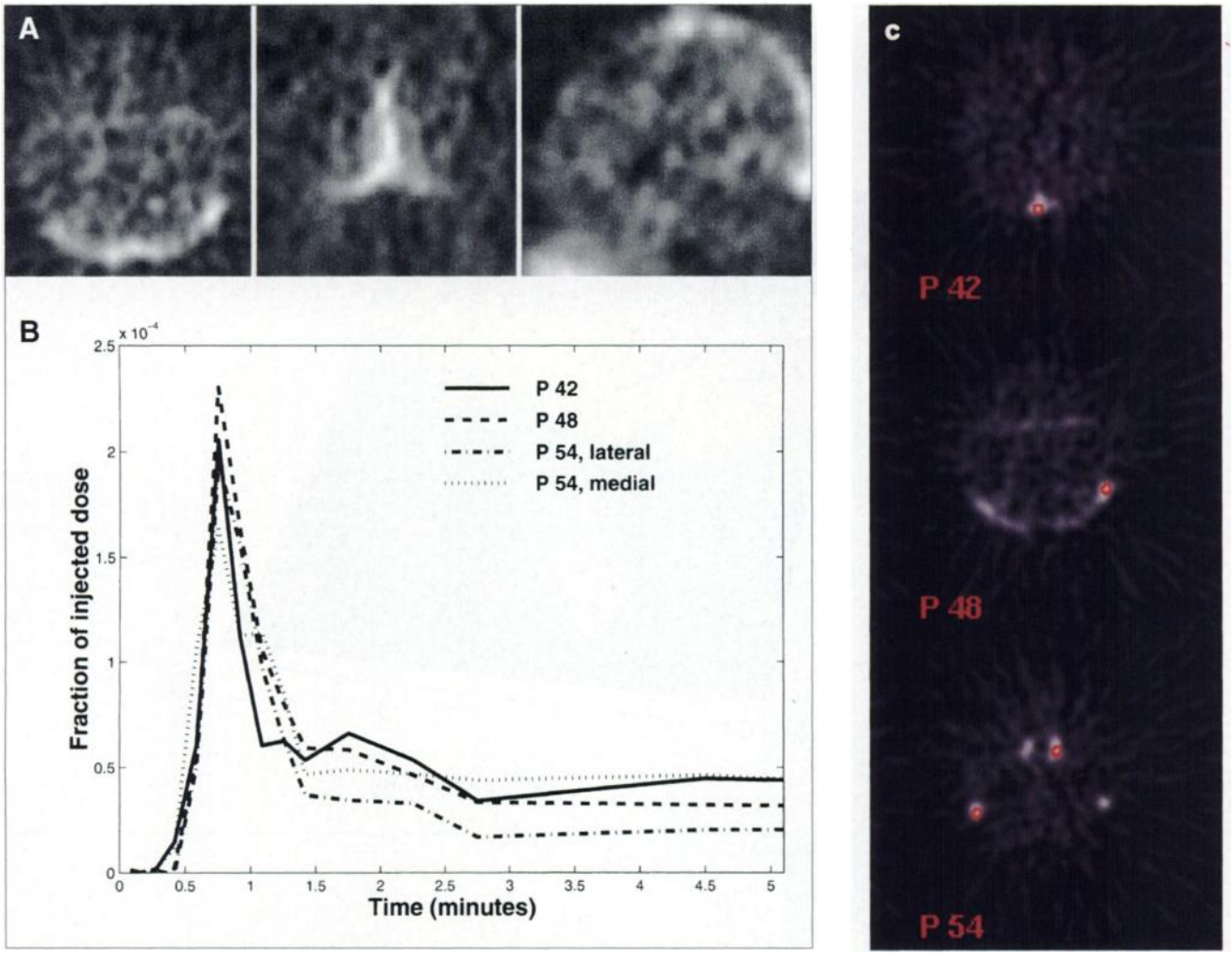

FIGURE 1. Intracranial blood pool. (A) Venous blood pool in transaxial (left), coronal (center) and sagittal (right) sections of FmT PET study is shown. Transverse and superior sagittal sinuses are clearly visible in these images. (B) Graph illustrates time courses of radioactivity in circular ROIs defined on transaxial sections (C). ROIs illustrated are 3.5 mm in radius and were defined at confluens sinuum (P 42), lateral aspect of left transverse sinus (P 48), intersection of right transverse and sigmoid sinuses (P 54, lateral) and left internal carotid artery (P 54, medial). Note that maximum value of peak height obtained in venous ROIs is 41% higher than peak value obtained in internal carotid artery. Sections for ROIs were obtained by reslicing image volume into 75 transaxial sections, each 2 mm in depth.

radii. The inset shows the variation of the recovery coefficient with region radius for vessel radii of 3, 4 and 5 mm. Note that the magnitude of f is about 0.5 but can vary between 0.3 and 0.7 for the region sizes used in this study, which were 3.5- to 5.5-mm radii. Figure 2B illustrates the excellent agreement we observed between this analytic model and the recovery coefficients we determined experimentally, particularly for small ROI radii and vessel radii between 3 and 6 mm. For larger vessels, the model slightly overestimates the recovery coefficient (Discussion).

To approximate the magnitude of the partial-volume effect for a given patient, we used the actual radius of the venous ROI for that patient and a fixed value of 4 mm for the radius of the blood pool at the confluens sinuum. The latter value was obtained by direct measurement of an MR venogram obtained in a healthy, 52-y-old man and compares well with scaled diagrams available in the literature (*32*). Some error is clearly introduced by assuming this value holds for all patients in this population; we examine this issue further in the Discussion.

The magnitude of the correction for partial volume and spillover changes over time, depending on the difference between activity in the ROI and activity in the surrounding tissue at each time point. We applied Equation 1 to the measured time course of radioactivity at the confluence of sinuses for each patient, using $C_o(t)$ for each patient as the time course of radioactivity in surrounding tissue. Figure 2C shows the mean amplitude of this correction for 25 patients, plotted as the difference between the measured $[C_m(t)]$ and corrected $[C_w(t)]$ curves at each time. Note that the correction for the recovery coefficient is highest at early times and falls to near zero after a few minutes. Also note that the maximum correction applied, on average, is about 1.25×10^{-4} of the injected dose, or 18% of the mean peak height of

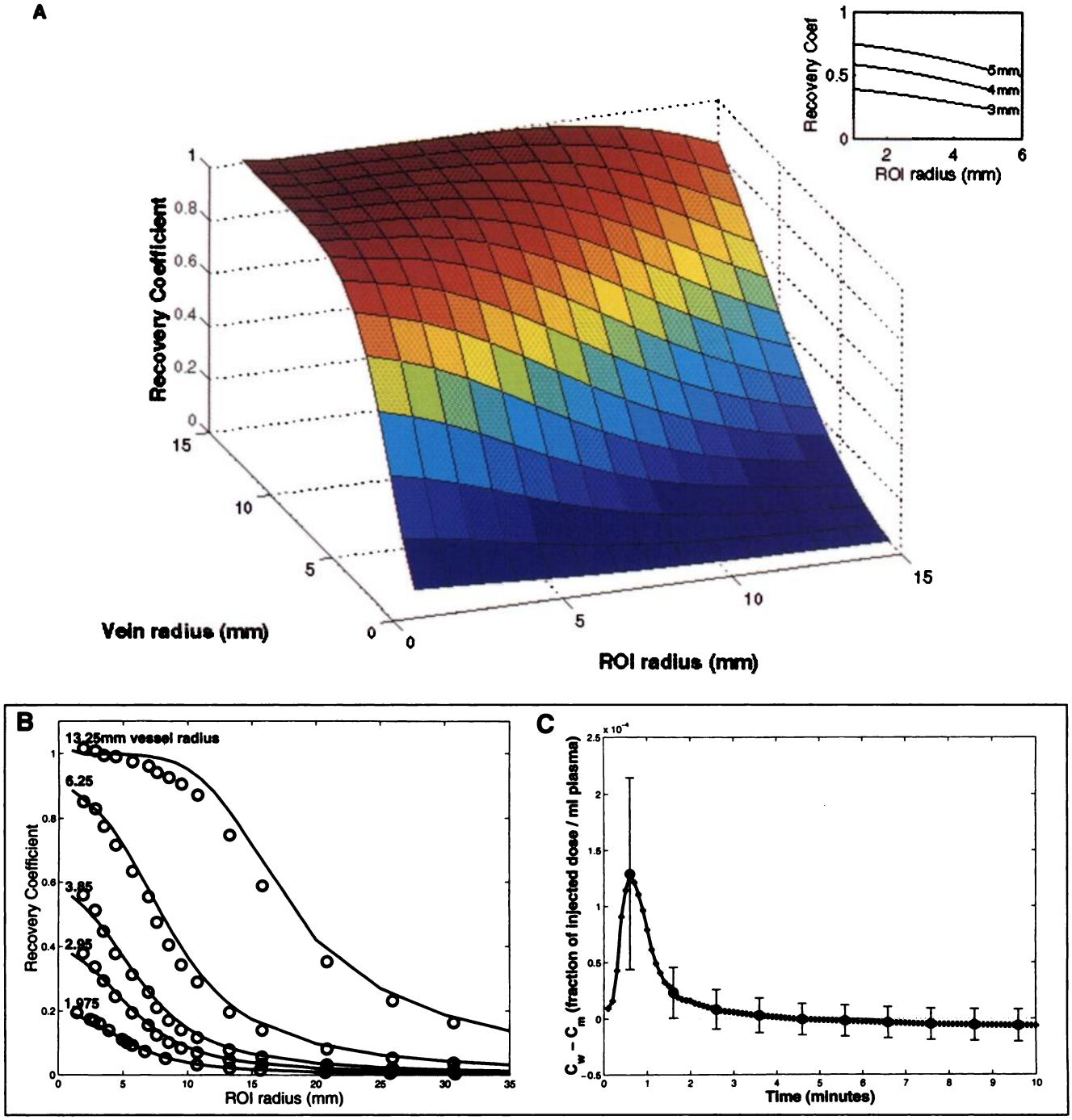

FIGURE 2. Partial-volume and spillover corrections. (A) Analytically determined recovery coefficient is shown for region of interest (ROI) and vessel radii between 1 and 15 mm. Inset shows recovery coefficient (Coef) for ROI radii between 1 and 5 mm and vessel radii of 3, 4 and 5 mm. (B) Analytically determined recovery coefficient (solid lines) for five vessel radii between 1.975 and 13.25 mm is compared with experimentally determined values (○). Note excellent agreement for small vessel and region radii. Divergence of calculated and measured values for large vessel radii may be associated with three-dimensional effects that were not included in analytic model. (C) Magnitude of mean partial-volume and spillover correction for 25 patients is shown. $C_w(t)$ = corrected curve; $C_m(t)$ = measured curve. Error bars illustrate ±1 SD. Note that correction is negligible after first 2 min.

$C_r(t)$ (see the following discussion of the results). The magnitude of this correction at the peak of $C_m(t)$ has a large SD because of intersubject differences in both peak height and time to peak.

Figure 3A shows the time course of radioactivity (expressed as fraction of injected dose per unit volume) in 1 mL plasma and 1 mL whole blood. Figure 3B illustrates the time course of the equilibration of radioactivity between plasma and red blood cells. The mean equilibration time constant for the 5 patients was 0.2346 min^{-1}. This value and a hematocrit

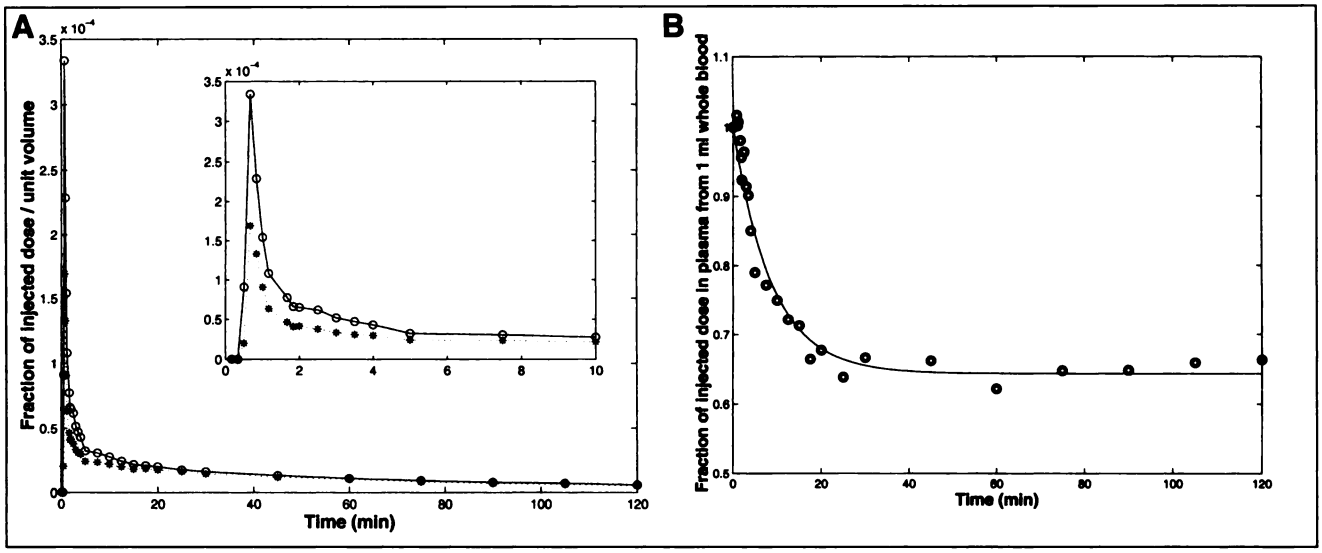

FIGURE 3. (A) Time course of radioactivity (fraction of injected dose per unit volume) in 1 mL plasma (○) and 1 mL whole blood (asterisks). Note expanded time scale in inset. (B) Fraction of counts in 1 mL whole blood that can be attributed to radioactivity in plasma at each time point. Solid line represents line of best fit to Equation 2.

of 0.42 for men (n = 16) or 0.38 for women (n = 9) were used in Equation 2 to obtain the concentration time course in the plasma contained in the venous input function.

Figure 4A shows the time course of radioactivity in whole blood determined by averaging ROI time courses for three ROIs defined at the confluence of sinuses on three successive image planes for a single patient. The time course of radioactivity in the venous ROI after correction for the recovery coefficient is plotted by the dashed line. Finally, the concentration time course of radioactivity in plasma is plotted by the solid line. The dot-dashed line shows the time course of radioactivity in sampled plasma for comparison.

After applying the partial volume and partition corrections, we were able to compare the sampled [$C_s(t)$] and ROI [$C_r(t)$] venous input functions. Table 1 gives the mean and SD of the peak height, time to peak and total integral under each of these curves. The ROI input function peaks significantly earlier (n = 25, t = 4.70, $\alpha < 0.001$) and higher (n = 25, t = 19.73, $\alpha < 0.001$) and has a smaller degree of intersubject variation. The peak height is plotted against time to peak for each patient in Figure 4B. These results highlight the greater degree of dispersion and delay that is intrinsic to the sampled venous input function. The total integral under the input function did not differ significantly between the two methods (n = 25, t = 1.06, $\alpha > 0.3$).

The mean sampled and venous input functions for all patients are shown in Figure 4C. As explained previously, we shifted each $C_s(t)$ to peak at 2.45 s and each $C_r(t)$ to peak at 0.66 s before computing the average. The sampled input function has clearly been subject to a far greater degree of dispersion and delay. The best fit of the mean $C_r(t)$ to the analytic function described in Equation 3 was given by $M' = 0.44\ mm^{-1}$, $D' = 8.67e\text{-}4\ s^{-1}$ and $v' = 2.48e\text{-}2\ s^{-1}$ and is shown by the solid line in Figure 4C. This function was fit to data points up to 1 min, before recirculation of the tracer is apparent. The deconvolution of this smooth fit with the arterial-venous transfer function for tyrosine is shown by the dashed line. This estimate of the arterial supply of FmT to brain tissue peaks at 28.7 s (0.48 min) and 0.075 %ID (7.5×10^{-4}) (compare with values in Table 1).

The results of graphic analysis using the metabolite-corrected input functions are shown in Table 2, which also provides the correlation coefficient, *r*, and the significance level of the *t* test, α. (Note that the value of α shown in Table 2 reflects the probability that there is a significant difference between the two distributions of K_i, not whether the correlation differs significantly from zero.) The correlation coefficient between influx constants obtained by the two methods was 0.69, and neither the values of K_i nor the graphic intercept determined by the two methods were significantly different at the 5% significance level (Fig. 5A). There appears to be a trend toward higher influx constants when calculated with the ROI input function, however, and for a greater degree of variation within our patient population.

The results of compartmental analysis are shown in a similar manner in Table 3. The values of all three rate constants calculated by the two methods were correlated. No significant differences were observed between the mean values of the rate constants determined using the two input functions, although there appeared to be a trend toward lower values of K_1 and k_2 when the ROI input function was used. The distribution of k_3 values that were determined using the two input functions is illustrated in Figure 5B.

DISCUSSION

Quantitative assessments of dopaminergic function (such as a K_i) are routinely requested for patient studies at our institution, and the need for quantitative clinical PET

therefore provided the impetus for this study. Recent reports in the literature (*8,10,14,16,33*) have offered a variety of elegant solutions to several problems associated with arterial sampling; however, few of these techniques are applicable to diagnostic PET studies. The use of a reference region (*12–14,34*) as an input function or simple ratio techniques (*35,36*) also offer noninvasive quantitation and are far less sensitive to noise and partial-volume effects than the method we propose here. The ability to measure the time course of radioactivity in the circulation, however, offers greater flexibility for a range of modeling approaches and does not depend on the existence of an appropriate reference region for each tissue or metabolic rate constant under study. For example, our experience with 3-O-methyl-6-^{18}F-fluoro-L-dopa, the methylated metabolite of 6-^{18}F-fluoro-L-dopa, indicates that this substance is handled differently by dopaminergic and nondopaminergic regions of the human brain (*37*).

TABLE 1
Comparison of Sampled Venous and Venous ROI Input Functions

Input function	Peak height* mean ± SD (SD/mean)	Time to peak (min) mean ± SD (SD/mean)	Total integral† mean ± SD (SD/mean)
$C_s(t)$, sampled	1.08 ± 1.05 (0.97)	2.45 ± 2.02 (0.82)	11.5 ± 4.9 (0.43)
$C_r(t)$, ROI	5.75 ± 2.21 (0.38)	0.66 ± 0.24 (0.36)	10.1 ± 4.5 (0.44)

*Units are fraction of dose injected; values shown are $\times 10^{-4}$.
†Units are (fraction of dose injected) × min; values shown are $\times 10^{-4}$.
ROI = region of interest.

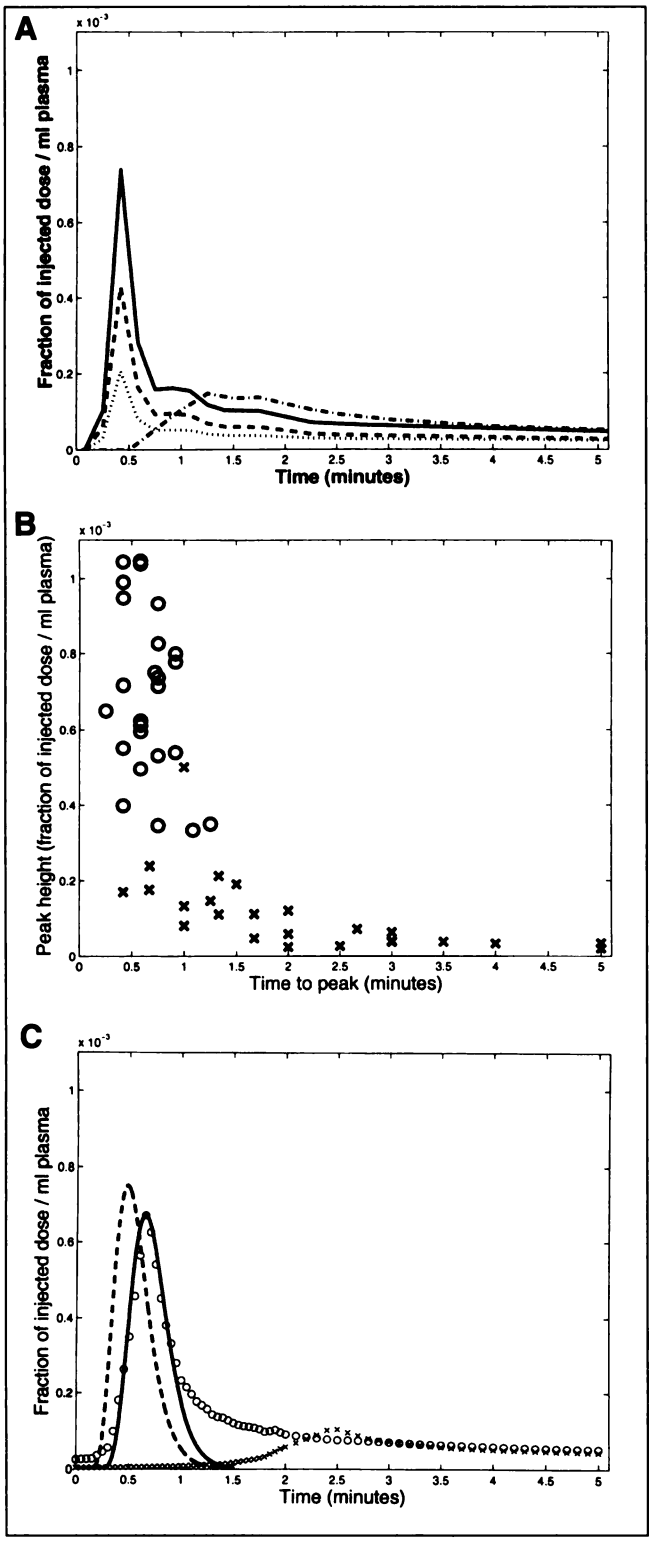

FIGURE 4. Comparison of sampled and ROI input functions. (A) Time courses of radioactivity in whole blood (dotted line), after partial-volume and spillover correction (dashed line) and after partition correction (solid line) for single patient. Dot-dashed line shows time course of radioactivity in sampled plasma for same patient. (B) Peak height versus time to peak for 25 patients in whom both venous ROI input function (○) and sampled venous input function (×) were obtained. (C) Mean time courses of radioactivity (n = 25) for venous ROI input function (○) and sampled venous input function (×). Solid line illustrates best fit of Equation 3 to first minute of mean ROI input function. Dashed line shows results of analytic model that predicts arterial time course of radioactivity, given measured venous time course. This estimate of arterial supply of tracer peaks 10.9 s earlier and 11% higher than venous ROI input function.

Figure 4A illustrates the disparity we observed between sampled and ROI input functions for a single patient. We were surprised to find this degree of dispersion and delay in the sampled input functions, given that the virtual transit time from the carotid to the radial artery is only 6.5 s (*28,38*). Koeppe et al. (*11*) showed that a single compartment was not adequate to describe the clearance of an inert, freely diffusable gaseous tracer from the hand, adding a further dispersion and delay, but this effect should be small. The dispersion of the sampled input function may be due in part to difficulties in obtaining blood samples rapidly from a clinical population, because venous samples often take close to 20 s to draw in these patients. The patient population had a

TABLE 2
Results of Graphic Analysis Using Sampled and ROI Input Functions

Input function	K_i (mL/min/mL) mean ± SD (SD/mean)	Intercept mean ± SD (SD/mean)
$\mathscr{C}_s(t)$, sampled	0.0133 ± 0.0080 (0.60)	2.01 ± 0.75 (0.37)
$\mathscr{C}_r(t)$, ROI	0.0211 ± 0.0153 (0.72)	1.51 ± 0.75 (0.50)
r	0.69	0.31
α	>0.10	>0.10

ROI = region of interest.

TABLE 3
Results of Compartmental Analysis Using Sampled and ROI Input Functions

Input function	K_1 (mL/min/mL) mean ± SD (SD/mean)	k_2 (min^{-1}) mean ± SD (SD/mean)	k_3 (min^{-1}) mean ± SD (SD/mean)
$\mathscr{C}_s(t)$, sampled	0.255 ± 0.256 (1.01)	0.153 ± 0.163 (1.06)	0.013 ± 0.004 (0.28)
$\mathscr{C}_r(t)$, ROI	0.103 ± 0.107 (1.04)	0.034 ± 0.027 (0.80)	0.014 ± 0.005 (0.37)
r	0.36	0.55	0.55
α	>0.05	>0.01	>0.5

ROI = region of interest.

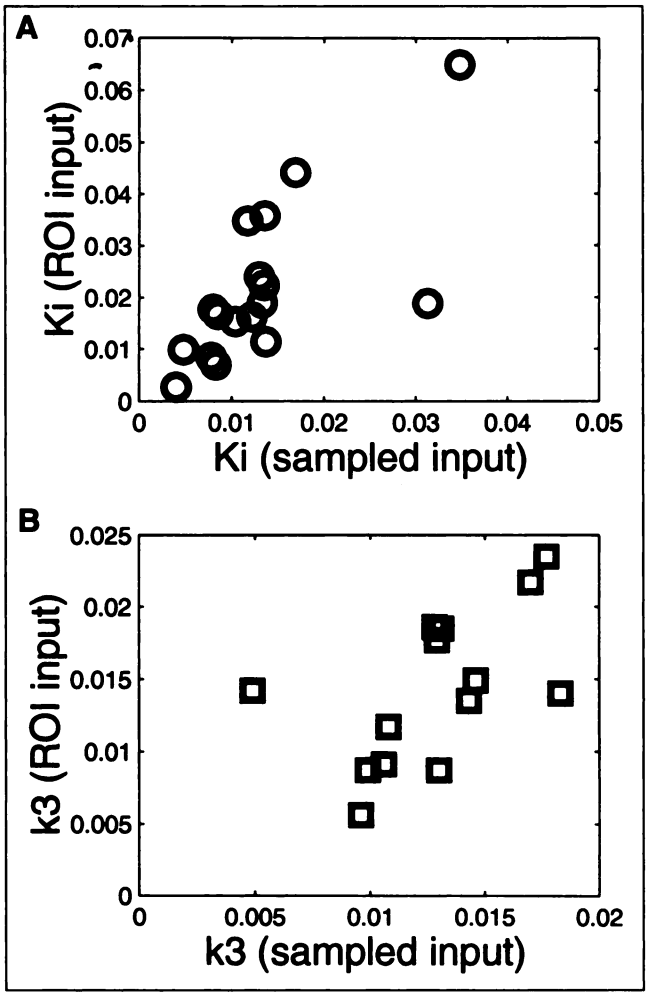

FIGURE 5. Results of graphic and compartmental analysis. (A) Influx constant, K_i (mL/min/mL), determined using region of interest (ROI) input function, is plotted against that determined using sampled input function; there was no significant difference between mean value of two distributions. (B) Parameter k_3 (min^{-1}), determined by compartmental analysis using two input functions, is shown. Again, differences in mean were not significant. We observed greater interpatient variation in both K_i and k_3 when ROI input function was used.

mean age of 53 y, and no exclusions were made in this study on the basis of cardiovascular disease, which is likely to be a further confounding issue. However, these patients are probably representative of those referred for investigations of cerebral dopaminergic function in a clinical PET department.

For those PET tracers, including FmT, for which peripheral metabolism of the injectate may influence quantitative results, a small number of venous blood samples (possibly only a single sample if population-based corrections are appropriate) must usually be obtained. This correction for peripheral metabolism is not unique to the technique presented, nor is it necessary for several PET tracers in current clinical use. Even though there is a need for metabolite correction when using the tracer FmT, we reduced the number of required blood samples from 38 to 5 through the use of a venous ROI input function.

The ROI input function is sensitive to the partition of the tracer between plasma and red blood cells. For example, in the case of fluorodeoxyglucose, the plasma and red blood cell radioactivities reach equilibrium rapidly, so that either the plasma or the whole-blood time-activity curves can be used as input functions (*15*). This is not the case with FmT (Fig. 3A). The red blood cell plasma membrane is permeable to several amino acids. Neutral aromatic amino acids, such as tyrosine, will enter the erythrocytes sharing a transport system with leucine that involves facilitated diffusion (*39*). We have presented an approach that includes the equilibration of the tracer between plasma and red blood cells. The results show that FmT equilibrium is reached in approximately 20 min (Fig. 3B).

We observed excellent agreement (within a few percent) between computationally and experimentally determined recovery coefficients for the vessel and region radii used in this study. The computational method of determining the recovery coefficient systematically overestimates f for very large vessel radii and may underestimate f for very small region sizes. These effects may be caused by the neglect of the axial dimension in our model; smoothing by the tomograph in the third dimension is ignored in the model. Figure

4A illustrates the difference, for a single patient, between the corrected and measured curves at each time point, that is, the magnitude of the partial-volume and spillover correction that was applied to the data in this example. Figure 2C shows the mean value of this correction for all patients; the peak height of the ROI input function is corrected by about 18% (with a large interpatient SD). From 2 min on, the difference is essentially equal to zero, so that the partial-volume and spillover correction has a negligible effect, that is, the corrected curve and the measured one are essentially the same. Although ideally an MR venogram would allow direct measurement of the dimensions of the confluence of venous sinuses in each patient, the error introduced by assuming a constant value for each patient is small; for vessel radii between 3 and 5 mm, the recovery coefficient varies between 0.3 and 0.7 (Fig. 2A). This implies that the true correction at the peak could be between 13% and 30% of peak height, whereas our estimate of a 4-mm vessel radius assumes a correction of 18%.

Our evaluation of more than 30 ROIs in the intracranial blood pools of 10 patients led us to position ROIs at the confluence of the superior sagittal, straight and transverse sinuses. This area of the venous blood pool is easily recognizable on the summed images from the first minute of an FmT study, providing an anatomic landmark to improve reproducibility, and has a volume that is large compared with that of other arteries and veins in the field of view. In addition, the position of this region of the blood pool within the skull allows an accurate attenuation correction to be performed analytically, obviating the need for measured attenuation correction and the subsequent increase in image noise that might be unavoidable if an inferior region were used. The use of ROIs defined over intracranial arteries to obtain an input function for PET has recently been proposed (*18*). In our experience, such regions have been prone to noise and have required large partial-volume and spillover corrections; this makes us somewhat cautious in recommending arterial ROIs for routine clinical use, particularly when modeling efforts may be sensitive to noise in the input function (*3–5,18*). The radius of the internal carotid artery, for example, is only 2.3 ± 0.4 mm (*40*), and therefore the diameter is smaller than the resolution of the tomographs (FWHM). An arterial ROI, however, may be feasible when using a tomograph with higher sensitivity or better resolution (or both) than those used in this study or when the modeling undertaken is relatively insensitive to noise in the input function.

The dashed line in Figure 4C illustrates the analytic estimate of the arterial supply of radiotracer to the brain. This curve peaks about 10 s before the venous ROI input function and has a peak height that is approximately 10% higher than $C_r(t)$. Although this arterial-venous dispersion is significant when compared with the exquisite accuracy now available for arterial sampling with tracers such as ^{15}O-labeled water, these differences are small when compared with $C_s(t)$, the sampled venous input function, and will likely have a minimal effect on calculated parameter values. Again, note that the dispersion and delay in the $C_s(t)$ does not reflect a normal population but reflects a group of patients with a mean age of 53 y. This analysis suggests that the venous ROI input function may be much closer to the arterial input to brain tissue than the arterialized venous input function obtained in a middle-aged or elderly clinical population. This analytic approach rests on the assumptions that sodium is a good reference tracer for amino acids (*28*) and that the transit of FmT through the brain will be similar to that of tyrosine.

Because the sampled and ROI input functions converge after initial differences in the early peak, the net influx of tracer, after the system reaches equilibrium, should be fairly insensitive to the input function used. This was confirmed in the graphic and compartmental analyses studied here (Tables 2 and 3); neither K_i (*18*) nor k_3 was significantly affected by the choice of input function. There appears to be a trend toward higher values of the rate constants K_1 and k_2 when determined using the sampled input function. This difference is associated with the lower peak height in the sampled input function: To achieve the same amount of tracer in tissue at early times, the flux of tracer into the reversible compartments must be higher if the input function is lower. The use of the ROI input function decreases the variance in parameters K_1 and k_2 while increasing the variance in K_i and k_3. This may indicate that the effects of interpatient differences in blood circulation and sampling have been reduced, whereas interpatient variations in dopaminergic function are now more readily quantified.

CONCLUSION

We present an alternative means of determining a plasma input function for PET studies, with the aim of increasing the feasibility of quantitative PET in busy clinical settings. We find that the sensitivity and resolution of current tomographs make a venous ROI-based input function possible, and we introduce simple corrections to this input function for partial volume, spillover and partition of the tracer between plasma and red blood cells. The investigations suggest that the venous ROI input function may be closer to the arterial supply of radiotracer to the brain than arterialized venous blood, at least in some patient populations.

ACKNOWLEDGMENTS

The authors thank Raman Chirakal for preparing the radiopharmaceutical used in this study, Jia Jun Chen for analysis of the plasma metabolites, Margo Thompson for untiring support and Susanne Kish, Chantal Landry, Mike Lepine and Sandy Upton for help with the data collection. The authors acknowledge the generous support of the Chedoke-McMaster Hospitals Foundation and the Natural Sciences and Engineering Research Council of Canada.

REFERENCES

1. Huang SC, Carson RE, Phelps ME. Tracer kinetic modeling in positron computed tomography. In: Lambrecht RM, Escigno A, eds. *Tracer Kinetics and Physiologic Modeling*. New York, NY: Springer-Verlag; 1983:298–344.
2. Meyer G-J, Waters SL, Coenen HH, Luxen A, Maziere B, Langstrom B. PET radiopharmaceuticals in Europe: current use and data relevant for the formulation of summaries of product characteristics. *Eur J Nucl Med.* 1995;22:1420–1432.
3. Kato A, Menon D, Diksic M, Yamamoto YL. Influence of the input function on the calculation of the local cerebral metabolic rate for glucose in the deoxyglucose method. *J Cereb Blood Flow Metab.* 1984;4:41–46.
4. Chen K, Huang SC, Yu DC. The effects of measurement noise in plasma radioactivity curves on model parameter estimation in positron emission tomography. *Phys Med Biol.* 1991;36:1183–1200.
5. Feng D, Huang SC, Wang X. Models for computer simulation studies of input functions for tracer kinetic modeling with positron emission tomography. *Int J Biomed Comput.* 1993;32:95–110.
6. Huang SC, Phelps ME, Hoffman EJ, Sideris K, Selin CJ, Kuhl DE. Noninvasive determination of local cerebral metabolic rate of glucose in man. *Am J Physiol.* 1980;238:E60–E82.
7. Wong W-H, Hicks K. A clinically practical method to acquire parametric images of unidirectional metabolic rates and blood spaces. *J Nucl Med.* 1994;35:1206–1212.
8. Feng D, Wong K-P, Wu C-M, Siu W-C. Simultaneous extraction of physiological and input function parameters from PET measurement. *Neuroimage.* 1997;5:B73.
9. Takikawa S, Dhawan V, Spetsieris P, et al. Noninvasive quantitative fluorodeoxyglucose PET studies with an estimated input function derived from a population based arterial blood curve. *Radiology.* 1993;188:131–136.
10. Eberl S, Anayat AR, Fulton RR, Hooper PK, Fulham MJ. Evaluation of two population-based input functions for quantitative neurological FDG PET studies. *Eur J Nucl Med.* 1997;24:299–304.
11. Koeppe RA, Holden JE, Polcyn RE, Nickles RJ, Hutchins GD, Weese JL. Quantitation of local cerebral blood flow and partition coefficient without arterial sampling: theory and validation. *J Cereb Blood Flow Metab.* 1985;5:214–223.
12. Patlak CS, Blasberg RB. Graphical evaluation of blood-to-brain transfer constants from multiple-time uptake data: generalizations. *J Cereb Blood Flow Metab.* 1985;5:584–590.
13. Logan J, Fowler JS, Volkow ND, Wang G-J, Ding Y-S, Alexoff DL. Distribution volume ratios without blood sampling from graphical analysis of PET data. *J Cereb Blood Flow Metab.* 1986;16:834–840.
14. Gunn RN, Lammertsma AA, Hume SP, Cunningham VJ. Parametric imaging of ligand-receptor binding in PET using a simplified reference region model. *Neuroimage.* 1997;6:279–287.
15. Gambhir SS, Schwaiger M, Huang S-C, et al. Simple noninvasive quantification method for measuring myocardial glucose utilization in humans employing positron emission tomography and fluorine-18 deoxyglucose. *J Nucl Med.* 1989;30:359–366.
16. Muzik O, Chugani D, Shen C, DaSilva E. Non-invasive imaging of serotonin synthesis rate using PET and [C-11]alpha-methyl-tryptophan in autistic children. *Neuroimage.* 1997;5:B16.
17. Lockwood AH. Invasiveness in studies of brain function by positron emission tomography (PET). *J Cereb Blood Flow Metab.* 1985;5:487–489.
18. Chen K, Bandy D, Reiman E, et al. Noninvasive quantification of the cerebral metabolic rate for glucose using positron emission tomography, ^{18}F-fluoro-2-deoxyglucose, the Patlak method, and an image-derived input function. *J Cereb Blood Flow Metab.* 1998;18:716–723.
19. Axel L. Tissue mean transit time from dynamic computed tomography by a simple deconvolution technique. *Invest Radiol.* 1983;18:94–99.
20. Perman WH, Gado MH, Larson KB, Perlmutter JS. Simultaneous MR acquisition of arterial and brain signal-time curves. *Magn Reson Med.* 1992;28:74–83.
21. DeJesus O, Mukherjee J. Radiobrominated m-tyrosine analog as potential CNS L-dopa PET tracer. *Biochem Biophys Res Commun.* 1988;150:1027–1031.
22. Chirakal R, Schrobilgen GJ, Firnau G, Garnett ES. Synthesis of 18-F labelled fluoro-*m*-tyrosine, fluoro-*m*-tyramine and fluoro-3-hydroxyphenylacetic acid. *Appl Radiat Isot.* 1991;42:113–119.
23. Nahmias C, Wahl L, Chirakal R, Firnau G, Garnett ES. A probe for intracerebral aromatic amino-acid decarboxylase activity: distribution and kinetics of [^{18}F]6-fluoro-L-*m*-tyrosine in the human brain. *Mov Disord.* 1995;10:298–304.
24. Cumming P, Gjedde A. Compartmental analysis of dopa decarboxylation in living brain from dynamic positron emission tomograms. *Synapse.* 1998;29:37–61.
25. Chen C-H, Muzic RF Jr, Nelson AD, Adler LP. A nonlinear spatially variant object-dependent system model for prediction of partial volume effects and scatter in PET. *IEEE Trans Med Imag.* 1998;17:214–227.
26. Oldendorf WH. Measurement of the mean transit time of cerebral circulation by external detection of an intravenously injected radioisotope. *J Nucl Med.* 1962;3:382–398.
27. Knudsen GM, Pettigrew KD, Paulson OB, Hertz MM, Patlak CS. Kinetic analysis of blood-brain barrier transport of D-glucose in man: quantitative evaluation in the presence of tracer backflux and capillary heterogeneity. *Microvasc Res.*1990;39:28–49.
28. Knudsen GM, Pettigrew KD, Patlak CS, Paulson OB. Blood-brain barrier permeability measurements by double-indicator method using intravenous injection. *Am J Physiol.* 1994;266:H987–H999.
29. Knudsen GM, Pettigrew KD, Patlak CS, Hertz MM, Paulson OB. Asymmetrical transport of amino acids across the blood-brain barrier in humans. *J Cereb Blood Flow Metab.* 1990;10:698–706.
30. Norwich KH. *Molecular Dynamics in Biosystems: The Kinetics of Tracers in Intact Organisms*. Oxford, England: Pergamon; 1977.
31. Wong DF, Gjedde A, Wagner HN Jr. Quantification of neuroreceptors in the living human brain. I. Irreversible binding of ligands. *J Cereb Blood Flow Metab.* 1986;6:137–146.
32. Carpenter MB, Sutin J. *Human Neuroanatomy*. Baltimore, MD: Wilkins & Wilkins; 1981:712.
33. Votaw JR, Shulman SD. Performance evaluation of the pico-count flow-through detector for use in cerebral blood flow PET studies. *J Nucl Med.* 1998;39:509–515.
34. Ishikawa T, Dhawan V, Chaly T, et al. Clinical significance of striatal DOPA decarboxlyase activity in Parkinson's disease. *J Nucl Med.* 1996;37:216–222.
35. Hoshi H, Kuwabara H, Léger G, Cumming P, Guttman M, Gjedde A. 6-[^{18}F]fluoro-L-dopa metabolism in living human brain: a comparison of six analytical methods. *J Cereb Blood Flow Metab.* 1993;13:57–69.
36. Vingerhoets FJG, Schulzer M, Ruth TJ, Holden JE, Snow BJ. Reproducibility and discriminating ability of fluorine-18–6-fluoro-L-dopa PET in Parkinson's disease. *J Nucl Med.* 1996;37:421–426.
37. Wahl LM, Chirakal R, Firnau G, Garnett ES, Nahmias C. The distribution and kinetics of [^{18}F]6-fluoro-3-*O*-methyl-L-dopa in the human brain. *J Cereb Blood Flow Metab.* 1994;14:664–670.
38. Raichle ME, Martin WRW, Herscovitch P, Mintun MA, Markham J. Brain blood flow measured with intravenous $H_2{}^{15}O$. II. Implementation and validation. *J Nucl Med.* 1983;24:790–798.
39. Tunnicliff G. Amino acid transport by human erythocyte membranes. *Comp Biochem Physiol.* 1994;108A:471–478.
40. Kane AG, Dillon WP, Barkovich AJ, Norman D, Dowd CF, Kane TT. Reduced caliber of the internal carotid artery: a normal finding with ipsilateral absence or hypoplasia of the A1 segment. *AJNR.* 1997;18:1595–1596.